Al-Nahrain Journal for Engineering Sciences (NJES) Vol.20 No.1, 2017 pp.222 - 234

Computational Fluid Dynamics (CFD) Modeling Study of Thermal Performance for Multipurpose Solar Heating System

Audai Hussein Al-Abbas
Pumps Eng. Department, Technical College of Al-Mussaib (TCM)
Al-Furat Al-Awsat Technical University

Abstract

The 3-D numerical simulations of the thermal collectors in solar heating systems were conducted to simulate the conventional solar heating system, multipurpose solar water heater (MPSWH), and multipurpose solar air heater (MPSAH). The commercial computational fluid dynamics (CFD), AVL Fire ver. 2009.2 was used to solve and investigate the temperature distributions in the absorber plate and riser tube of both solar water and air heater during summer and winter seasons. The RNG k - ε turbulence model was employed for this CFD study. The present paper was to provide a good understanding of thermal performance for the solar collector at different operating conditions. The experimental setup and physical data of Venkatesh, R. and Christraj, W. [15] were employed as geometric parameters and initial boundary conditions to model and to validate the predicted numerical values. Comparing to the values of temperatures for the conventional SWH and SAH, the predicted results of the MPSWH and the MPSAH showed a good improvement on the thermal performance. These enhancements on the temperature may have been due to the new design adopted in the multipurpose solar heating systems by using riser tubes and headers to the original design of the thermal systems. Additionally, the thermal performance of solar collectors increases with increasing the mass flow rates and thermal conductivity of absorber plate. For validation aspect, the predicted results of all cases examined showed a good agreement against the measured results in terms of temperature distribution levels and thermal efficiencies.

Keywords: Solar collector, CFD simulation, solar water heater, Solar air heater.

1. Introduction

In order to gradually move from the conventional sources of energy to renewable energy sources, solar thermal technology has a great

Importance to be widely used. Solar energy is an abundant, but capturing process is not low-priced. It remains many times expensive than those produced from firing the fossil fuels in thermal power plants. For those reasons, research, innovation, and development in this sector of clean energy is highly required to be built. However, the common applications of solar energy are solar water heating and solar air heating. Solar water heating (SWH) is largely used in many developed countries worldwide. Solar energy conversion is a natural and secure, and it is cost-effective process to collect hot water by using solar radiations. Solar air heating (SAH) is a simple device to heat air by using solar energy comparing with solar water heating devices because of minimal usage of required system components, and the direct use of air as a working fluid [1-5].

Nowadays, the dynamic thermal behavior of flat plat solar collectors have been numerically developed using several numerical models. Computational fluid dynamic (CFD) codes have been widely used to model these solar thermal collectors in order to obtain a better physical understanding about the thermal behavior and to optimize these solar systems. Generally, the CFD tool is concerned to solve non-linear partial differential equations which describe the behavior and phenomenon of fluid dynamic. The governing equations are basically derived from the conservation of mass, momentum, and energy equations so as to represent any engineering problems in heat and mass transfer fields [6 and 7].

Zima and Dziewa [8 and 9] analyzed the inertia effects to glass cover, insulation, and air gap by using a one-dimensional 5n-node method. An implicit finite difference (FD) approach used to characterize and solve two different ordinary differential equations which are described two different temperature-dependent parameters. The first model employed to work for steady state condition because of inertia effect, whereas the second mathematical model was taken into consideration the effect of the heat transfer characteristic by combining the thermal power on the surface and the heat capacity of fluid. The results of model were validated against the obtained results from the analytical solution and showed a good agreement under the transient conditions.

A TRNSYS code was used to simulate and investigate the performance of water-in-glass evacuated tube solar water systems by Budihardjo and Morrison [10]. Several geometrical engineering parameters, such as tank size, angles, numbers of tubes and locations, were considered and modeled to investigate the effect of thermal inertia on the solar water heating system. The results showed that the thermal performance of a typical 30 tube evacuated array is lower than that of panel thermal flat plate array for domestic water heating system.

In the same trend of the numerical approach, Ayome et al. [11] employed a TRNSYS code to calculate the effect of circulating heating system with flat plate and evacuated tube collector for quasi-state conditions. The accuracy of predicted results was higher than 80 percent for the outlet water temperature, and this developed model can be beneficially used for high duration performance of solar thermal systems with different conditions and at different locations.

A commercial CFD Fluent code ver. 6.1 was used by Fan et al. [12] to investigate and analyze the flow distribution in a solar collector panel with inclined absorber strips. A uniform energy generation in the absorber and the coefficient of convective heat loss were only assumed during modeling the thermal collector. For high mass flow rates, a good agreement was achieved between the predicted results and the experimental results, while for low flow rates the comparisons showed some deviations.

Turgut and Onur [13] employed the CFD software Fluent ver. 6.3 to study the effect of forced convection heat transfer on the surface of flat plate thermal collector. Their experimental results, which were focused on finding the dimensionless empirical correlation, were compared against the CFD results, and showed small discrepancies for heat transfer coefficient.

There are a few number of research work conducted on the solar water heating and solar air heating systems, particularly on the absorber plate and riser tube of the thermal collector. This means that the present investigations have been made based on the new design compared with the traditional device. The objective of this research work is to focus on the numerical simulation, using CFD, to provide a good understanding of the effect of operating and design parameters on thermal performance for the solar collector at different times. The idea is to provide useful information towards future modeling of long-term solar heating systems. In the present study the numerical modeling of multipurpose solar heating system (MPSHS) is carried out by using AVL Fire ver. 2009.2 CFD code [14], which is based on the finite volume method. The MPSHS was experimentally set up and conducted by Venkatesh and Christraj [15], as will be briefly reviewed in the next section. The validation was carried out against the experimental data [15] for the distributions of the water outlet temperatures and air outlet temperatures, and thermal efficiency over the time. Also, the mass flow rates and various absorber materials were investigated and presented for both the MPSWH and MPSAH in summer and winter seasons.

2. A Review of Experimental Set up of Venkatesh and Christraj[15]

The experimental setup of multipurpose solar heating system (MPSHS) for the natural convection mode of Venkatesh and Christraj was chosen for this simulation study to obtain a better physical understanding for solar heating systems under different operating parameters. The collector of multipurpose solar was designed by adding the solar water heater (SWH) and solar air heater (SAH). The riser tubes were added to the conventional solar water collector as modified parts with header. Four non-returned valves were used to make the system works as conventional solar collector and multipurpose solar collector. The latter can be worked as a SWH in winter and as a SAH during summer season. This collector consists of cover glass with an absorber plate, and it is connected to an insulated storage tank of 100 liters. In the MPSAH, the dimension of the device was 1070 mm length and 1070 mm width, and it consists of insulation material, transparent cover, absorber plate, storage tank, and air passage. Fig. 1a and b shows the schematic layout and photograph of solar water heater cum air heater with storage tank.

3. Mathematical Models and computational Methodology

The commercial CFD code, AVL Fire ver.2009.2, was selected to solve mathematical equations using the finite-volume technique in different 3-D unstructured grid systems. The solution algorithm employed in the CFD code is forceful and enables flexibility in the usage of any structured and unstructured grids. The finite-volume approach is different from other numerical methods (e.g. FEM and FDM) in terms of discretisation method and

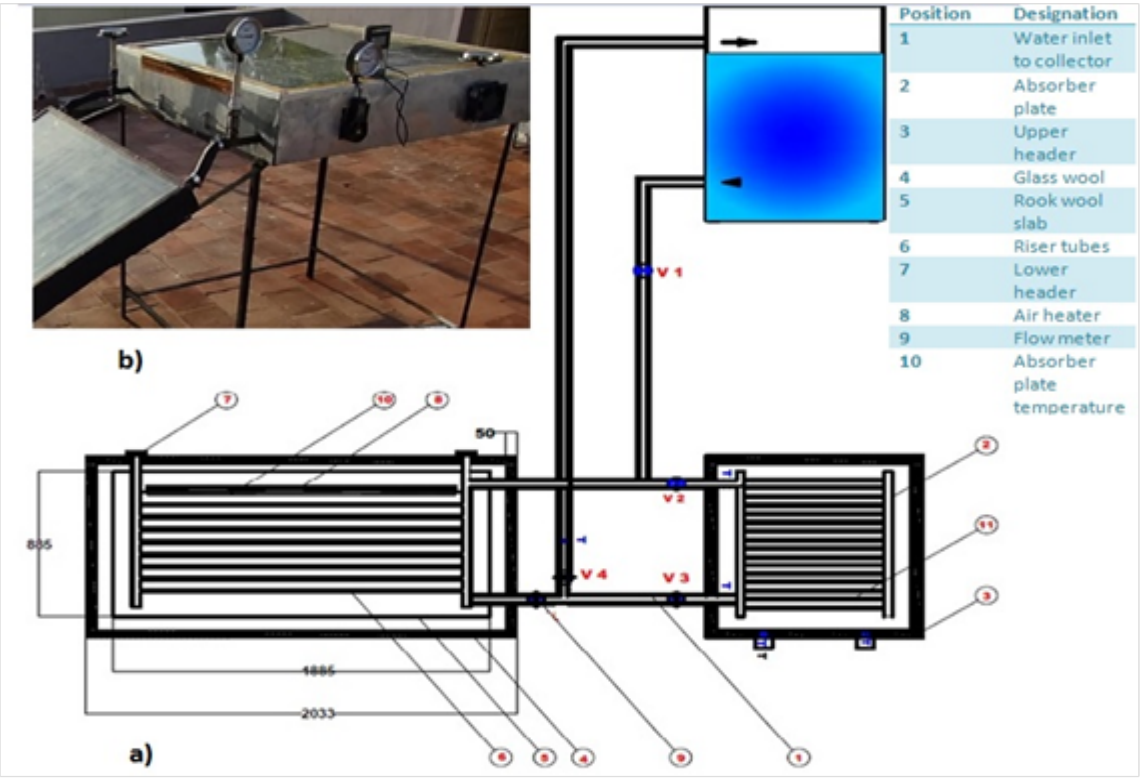

Figure 1: a) The schematic diagram of the solar water heater with storage tank (adopted from [15], all dimensions are given in mm), b) The photograph of multipurpose solar heating system.

Numerical solution: Both the laminar and turbulent flow models were considered and taken into calculations based on the operating conditions of the experiments. The RNG k - ε model has been implemented for turbulent flow modeling. The conduction heat transfer in glass cover and between the absorber plate and tubes were taken into consideration. The flow of the working fluid is also considered in the simulation. For the radiative heat transfer in the computational domain, the radiative transport equation (RTE) has been used. This is employed to solve the heat transfer between the cover glass and the absorber plate. In the convergence criterion, the normalized absolute residuals for all the variables in each cell have been limited to be less than 10^{-4}. A first-order upwind scheme is employed for momentum, turbulent, and energy equations.

3.1 Governing Equations

The governing equations of mass conservation, momentum, and energy equations in the steady state conditions have been solved in the Cartesian tensor form:

- Mass conservation equation

$$\frac{\partial \rho}{\partial t}+\frac{\partial}{\partial x_i}(\rho u_i)=0 \quad \ldots (1)$$

- Momentum conservation equation

$$\frac{\partial}{\partial t}(\rho u_i)+\frac{\partial}{\partial x_j}(\rho u_i u_j)=-\frac{\partial P}{\partial x_i}+\frac{\partial}{\partial x_j}(\tau_{ij}) + \frac{\partial}{\partial x_j}\left(-\overline{\rho u_i' u_j'}\right) \quad \ldots (2)$$

- Energy equation

$$\frac{\partial}{\partial t}(\rho E)+\frac{\partial}{\partial x_i}[u_i(\rho E+P)]= \frac{\partial}{\partial x_j}\left(k\frac{\partial T}{\partial x_j}+u_i(\tau_{ij})\right)+S_\phi \quad \ldots (3)$$

Where $\mathbb{P}$ is the pressure of fluid, u_i and u_j are the velocity components in the ith and jth directions, respectively. ϕ denotes internal energy, while term S_ϕ represents the appropriate source of the variables ϕ.

These equations can be used with approximations according to the properties of turbulent fluid flow to provide approximate averaged solutions to the Navier-Stokes equations. For an incompressible fluid flow, these mathematical equations can be given as[16]:

$$\frac{\partial}{\partial X_j}\left(\overline{u_i u_j}\right) = \frac{-1}{\rho_f}\frac{\partial \bar{P}}{\partial X_i} + \frac{\partial}{\partial X_j}\left[\mu_{eff}\left(\frac{\partial u_i}{\partial X_j} + \frac{\partial u_j}{\partial X_i}\right)\right] \quad \dots (4)$$

Where: $\mu_{eff} = \mu + \mu_t$, $\mu_t = C_\mu \frac{\kappa^2}{\varepsilon}$, $C_\mu = 0.0845$, K= 0.71 $\varepsilon^{2/3} L^{2/3}$

The values of k and ε are determined via transport equations:

$$\bar{u_i}\frac{\partial k}{\partial X_i} = v_t S^2 - \varepsilon + \frac{\partial}{\partial X_i}\left(\alpha_t v_t \frac{\partial k}{\partial X_i}\right) \quad \dots (5)$$

And

$$\bar{u_i}\frac{\partial \varepsilon}{\partial X_i} = \frac{C_{\varepsilon 1}\,\varepsilon\, v_t}{k} S^2 - \frac{C_{\varepsilon 2}\,\varepsilon^2}{k} - R + \frac{\partial}{\partial X_i}\left(\alpha_t v_t \frac{\partial \varepsilon}{\partial X_i}\right) \quad \dots (6)$$

The parameter α_t is inverse Prandtl number for turbulent transport. The turbulent viscosity v_t is as follows [17]:

$$v_t = \left(v_{eddy} - v_o\right) \quad \dots (7)$$

R is given by:

$$R = \frac{C_\mu \eta^3 \left(1 - \eta/\eta_0\right)}{1 + \psi \eta^3}\frac{\varepsilon^2}{k} \quad \dots (8)$$

The values of above-mentioned constants are given below [18]:

$\eta = S\,k/\varepsilon$, $\eta_0 = 4.38$, $C_{\varepsilon 1=1.42}$, $C_{\varepsilon 2=1.68}$, $\alpha_{t=1.39}$, $\psi = 0.012$

The radiative transfer equation (RTE) is very convenient to describe the radiation phenomena in participating media due to the sum of contribution of all rays crossing the cell. The discrete ordinate (DO) model is activated to take the effect of heat transfer between the cover glass and absorber plate. The number of rays and their directions, which is chosen in RTE, is solved for each ray on its way from boundary to boundary. The general basis of this method is that the absorption coefficient and the temperature are assumed constant within a single control volume. The heat radiation intensities at connections of cells can be calculated over the total spectrum as given below [19]:

$$i'_{n+1} = i'_n\left(1 - \varepsilon\left(T, x_i\right)\right) + i'_b\left(T\right)\varepsilon\left(T, x_i\right) \quad \dots (9)$$

Where $\varepsilon\left(T, x_i\right)$ represents the emissivity, $i'_b = \sigma \cdot T^4 / \pi$ is the blackbody radiation intensity in the control volume, and σ is the Stephan–Boltzmann constant that is equal to 5.67 × 10^{-8} W/m^2 K^4 .

Regarding the thermal efficiency, the solar collector efficiency, which is the ratio of stored energy in the storage tank to the total solar radiation (I_t) on the collector, has been calculated by [20]. The energy absorbed is related to the mass ($\dot{m}$), specific heat (C_p) and differences in temperatures between initial and final temperatures of fluid flow. The instantaneous thermal efficiency can be given as follows:

$$\eta_{th} = \dot{m} \cdot C_p \cdot \left(T_o - T_i\right) \Big/ \left(A_t \cdot I_t\right) \quad \dots (10)$$

3.2 Grid Independency Test

A grid independency is used as a scaling test to determine minimum grid resolution required to generate a solution, which is independent of the grid used. The 3-D computational domain of SWH was 200 mm height, 885 mm width, and 1885 mm length. While the domain of SAH was 200 mm height, 1035 mm width, and 1035 mm length as shown in Fig. 2. Three different non-uniform cell sizes (775412, 1244165, and 2665001 control volumes) were successively used for the calculations in the MPSWH case. Also, three different grid systems (629005, 1035972, and 2219052 control volumes) were tested in the calculations of the MPSAH case. The mean values of water outlet temperatures and air outlet temperatures over the time (see Table 1) were used for this purpose. The differences between the predicted temperatures and the experimental data for both the MPSWH and MPSAH examined cases were very marginal (see Figures 3 and 4). In addition, the percentage errors in the mean temperature distribution for these six grid systems were within 1%. Thus, the numerical solutions were essentially not sensitive to the number of cells and all the grid systems for the MPSWH and the MPSAH can provide same results. Therefore, it is

found that 1244165 and 1035972 cells for the MPSWH and the MPSAH, respectively are more sufficient, and these selected grid systems can reduce the computational time.

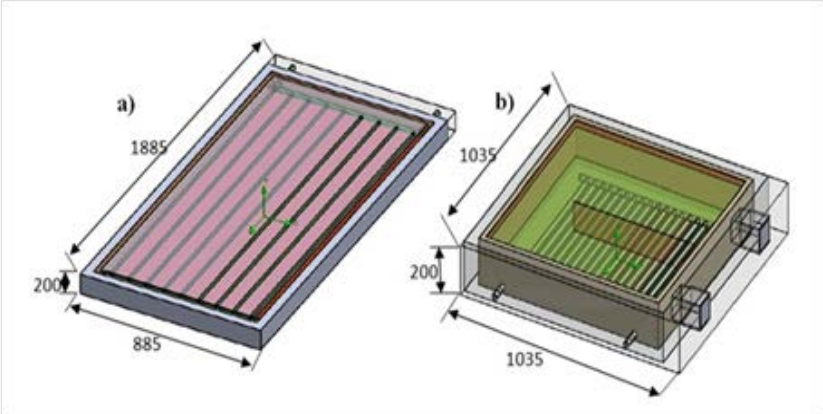

Figure 2: a and b: a) The 3-D computational domain of SWH, b) The 3-D computational domain of SAH, all dimensions are given in mm.

Table 1: Grid independency test.

CFD Models	No. of cells	$T(K)_{mean}$	Percentage error of ΔT_{mean}
MPSWH	755412	341.126	-
	1244165	339.036	0.61
	2665001	343.392	-1.2
MPSAH	629005	321.705	-
	1035972	319.142	0.79
	2219052	324.537	-1.6

3.3 Boundary Conditions

This subsection explains the boundary conditions applied on the computational domain of the MPSHS used in this simulation. First of all, the fluid flow is assumed to be steady and fully-developed flow. To simplify the numerical problem the radiation heat losses are neglected and the fluid flow assumed to be incompressible. The inlet conditions are taken from the experimental data [15], which has a set of different operating conditions such as inlet temperatures, mass flow rates, and modified solar radiation intensity. Table 2 includes the values of variables used in this study for the MPSWH and the MPSAH. The detailed descriptions of the MPSWH and the MPSAH are illustrated in Table 3. The direction of flow was along the axis of the tube. The thermo-physical properties such as the temperature, thermal conductivity, and density of fluids are taken into consideration of calculations. For the wall surfaces, non-slip condition was applied. The heat conduction for the absorber and riser tube was computed using shell conduction approach.

The transient heat flux parameter was employed in order to take the effect of heat generation on the surface of the absorber plate. The SIMPLE algorithm was used to solve the combinations between the velocity and pressure. A zero gradient was applied to the exit plane. The values used for the absorber absorptivity and glass trans missivity of the flat plate solar collector were 0.95 and 0.91, respectively.

4. Results and discussion

For validating the present CFD model, Fig. 3 a and b shows the comparison of the water outlet temperatures for MPSWH versus time between the experimental and predicted CFD results in summer and winter seasons, respectively. For all validation

Table 2: The values of mass flow rates, inlet temperatures, outlet temperatures, ambient temperatures, and solar intensity for the MPSWH and MPSAH at summer and winter seasons.

Description	MPSWH (summer)	MPSWH (winter)	MPSAH (summer)	MPSAH (winter)
Collector mass flow rate (kg/s)	0.0261	0.0231	0.0152	0.0143
Average inlet temperature (^oC)	51.60	37.82	60.16	46.14
Average outlet temperature (^oC)	57.86	41.76	68.62	48.24
Ambient temperature (^oC)	36.54	31.50	34.23	27.64
Average solar intensity (W/m^2)	1043	646	1007	663

Table 3: The model details for the MPSWH and the MPSAH.

Description	MPSWH	MPSAH
Aperture	2m x 2m	1m x 1m
Gross collector area	2035mm x 1035mm	1070mm x 1070mm
Working fluid	Water	Air
Absorbing material	Copper	Aluminum
Rear plate	Aluminum	Galvanized Iron

Tests, the real time used in this CFD modeling was higher than 480 minutes according to the experiments. It can be clearly seen that the panels a and b of Fig. 3 illustrate the same trend of temperature distribution over time. This means that the predicted results of water temperatures have approximately the same behavior against the experimental data. The CFD results revealed that the comparisons were within the acceptance limits. In summer season, the discrepancy falls within 9.46%, while during winter the difference was 8.31%. These predicted results are highly accepted in CFD community over the world based on the published numerical research works found in open literature

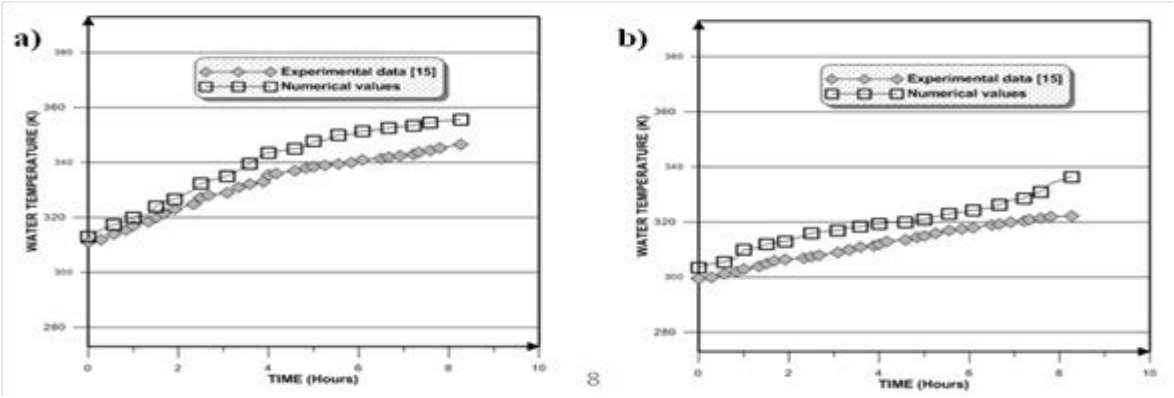

Figure 3: Temperature distribution profiles between the experimental and numerical results versus time of the MPSWH during (a) summer season and (b) winter season.

The comparisons of the air outlet temperatures for the MPSAH versus time between the experimental and predicted CFD results during the summer and winter seasons are presented in Fig. 4 a and b, respectively. As seen, both the experimental and CFD results illustrated the same trend of temperature distributions over the time, and this is numerically due to taking the effect of heat generation on the surface of the solar plate via using the transient heat flux parameter in CFD calculations. In the panel a of Fig.4, the numerical values of the air outlet temperature distributions showed a good agreement with the experimental data, and the deviations were 6.54%. But, in panel b the overall deviation between the numerical results

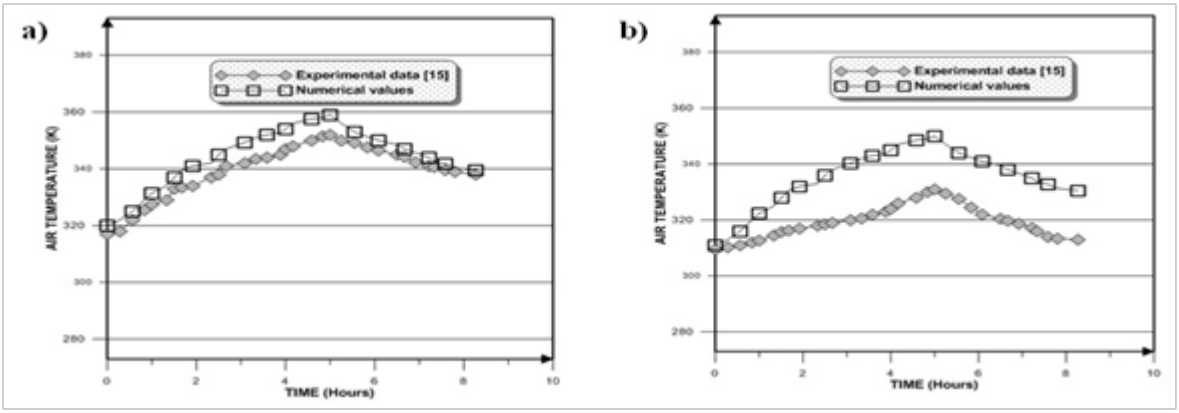

Figure 4: Temperature distribution profiles between the experimental and numerical results versus time of the MPSAH during (a) summer season and (b) winter season.

Results and physical data was less than 10.84%. These deviations may have been due to the numerical schemes and the turbulence model used and/or the uncertainties of experiments. However, this validated CFD model of solar heating systems can provide valuable information towards future numerical modeling of long-term solar heating systems under different operating conditions.

The first model of the present simulation was carried out during the summer season for the conventional solar water heater (SWH) and the

Conventional solar air heater (SAH). This simulation was performed based on the dimensions of the conduct experiments and initial conditions of operating parameters. In Fig. 5a and b, the distributions of the simulated temperatures are presented at the mid cut of the X-Z plane for the conventional SWH and the conventional SAH, respectively. It can be seen in Fig 5a that the highest simulated temperature of the thermal collector was 343.65 K for the conventional SWH. In Fig. 5b the highest temperature of the thermal collector was 335.83 K for the conventional SAH.

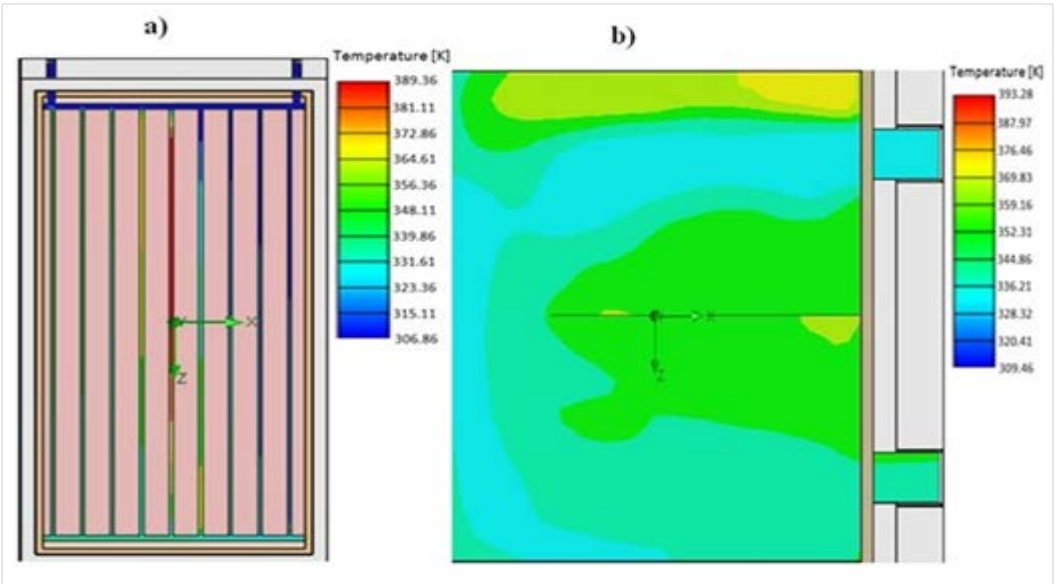

Figure 5: Distributions of simulated temperatures (K) at mid cut of X-Z plane for (a) the conventional SWH and (b) the conventional SAH.

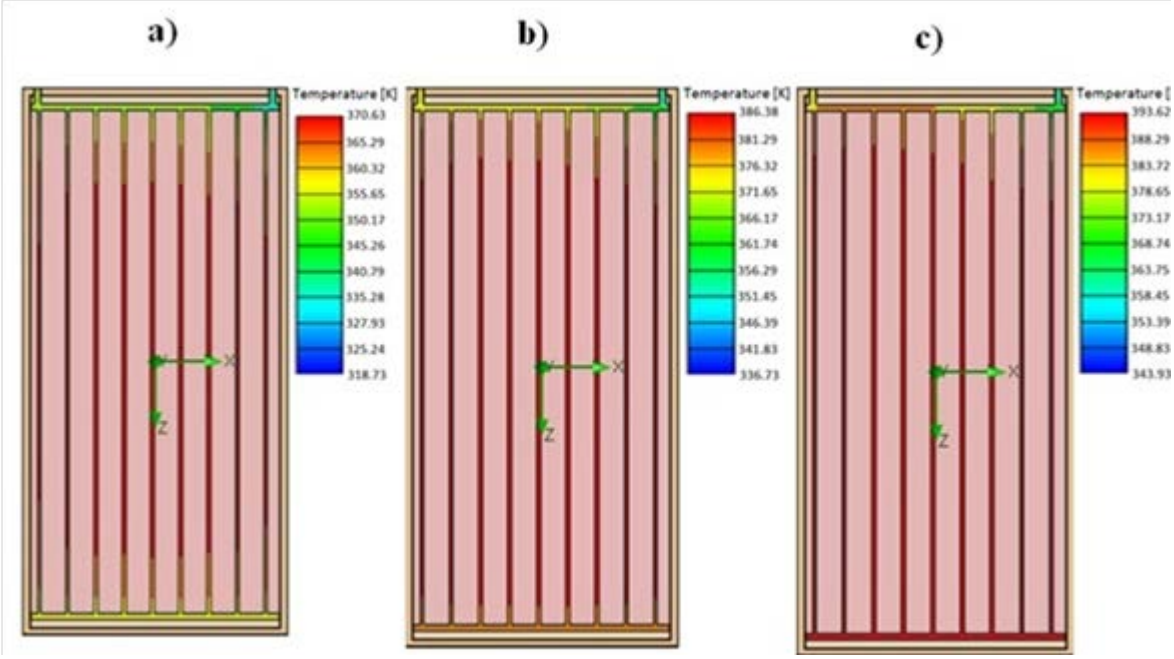

Figure 6: Distributions of simulated temperatures (K) of the MPSWH in summer season at different time (a) 11:30, (b) 13:30, and (c) 15:30 hours.

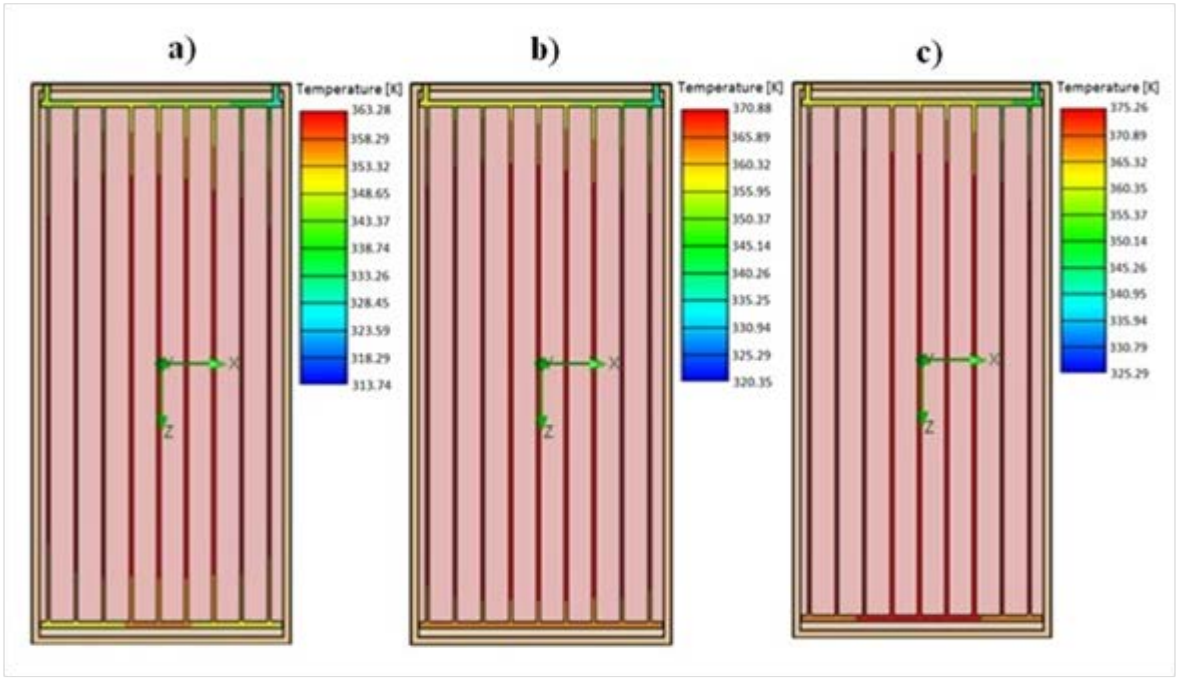

Figure 7: Distributions of simulated temperatures (K) of the MPSWH during winter season at different time (a) 11:30, (b) 13:30, and (c) 15:30 hours.

The temperature distributions of the MPSWH achieved from the predicted results during summer season at different times (11:30, 13:30, and 15:30 hours) are presented in Fig. 6. As seen, the temperature of the storage tank is gradually increased with increasing time. This increase in the temperature led to improving the thermal efficiency of the solar collector afternoon. The highest value of the temperature produced was around 381 K, as shown in panel c of Fig. 6. Fig. 7 shows the temperature distributions of the MPSWH at various times (11:30, 13:30, and 15:30 hours) in winter. The mass flow rates used in the simulation during both seasons were identical based on the experimental data, as given in Table 1. The highest temperature was about 369 K. As a result, there is a clear improvement on the temperature of the collector with respect to the conventional SWH, as mentioned earlier. This might be happened due to adding heat energy obtained in the storage tank with the riser tubes and headers.

Fig. 8 illustrates the temperature profile of the MPSAH for the absorber plate with riser tube. Both the convection and conduction heat transfer mathematical models were considered and taken into account in order to precisely analyze the thermal parameters. The highest value of the air temperature was 361 K, and it was close to the surface of the plate that leads to transfer the gained heat to the air in the air heater. Comparing to the maximum temperature of the conventional SAH, the CFD result revealed that the temperature of MPSAH is evidently high. That is undoubtedly occurred because of adding the heat energy of the riser tube to that of the air heater at midday time.

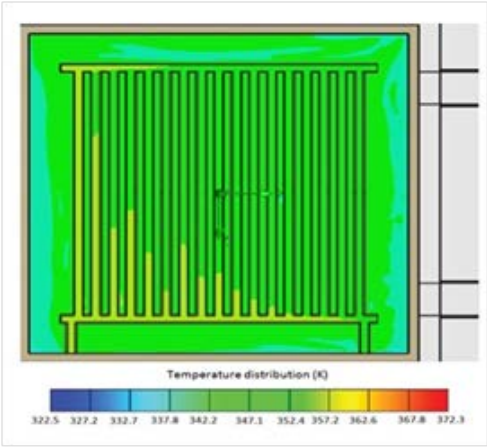

Figure 8: Distributions of simulated temperatures (K) of the MPSAH for the absorber plate with riser tube

Using CFD analysis, the velocity profile of MPSAH was obtained for the different mass flow rates of air. Fig. 9 shows the output of variation in the air velocity across the surface. It is observed from the Fig. 9 that the velocity profile is not resistance to high heat transfer rate from the surface of riser tube which is fitted below the absorber surface.

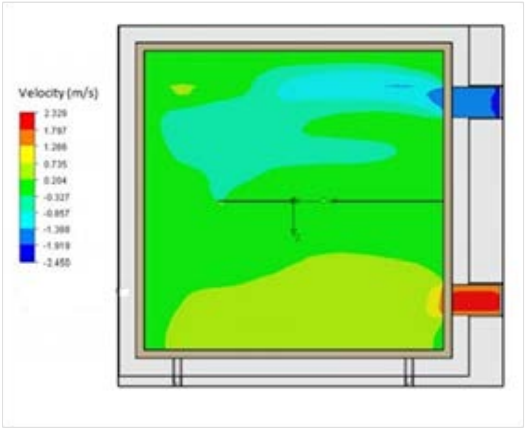

Figure 9: The output of variation in the air velocity across the surface

In order to increase the level of confidence of the present CFD model against the physical data, the thermal efficiencies have been compared as well. The maximum thermal performance efficiency of the multipurpose solar air heater at load condition during summer and winter in CFD analysis was registered as 80.15% and 73.86% for the mass flow rate of 0.0093 kg/s and 0.0176 kg/s, respectively. The comparison between experimental and simulated thermal efficiency of multipurpose solar air heater during summer and winter season is shown in Figures 10 and 11, respectively.

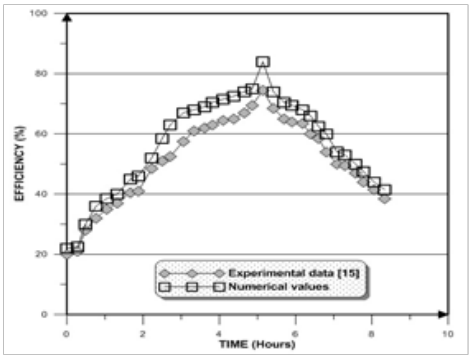

Figure 10: Comparison between experimental and simulated thermal efficiency of MPSAH during summer season.

It is noted that there is a sudden increase in the efficiency at around 5.8 hour and this is due to the increase in the average solar intensity at this time of the day and led as result to raise the outlet temperature of the fluid. The range of thermal performance is lower in a conventional solar air heater compared to a multipurpose solar air heater due to the absence of energy transfer from the water heater. In general, the predicted results illustrated the same trend of the experimental data over time.

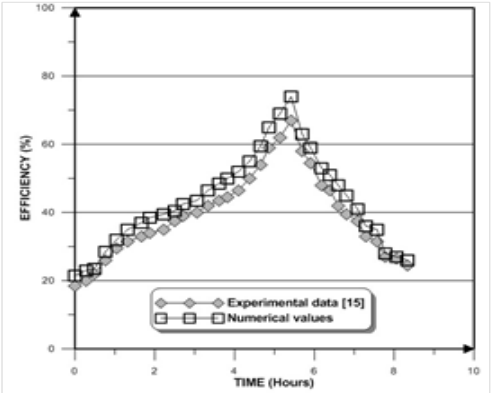

Figure 11: Comparison between experimental and simulated thermal efficiency of MPSAH during winter season

In order to take the effect of mass flow rates on thermal efficiency, Fig. 12 and Fig. 13 were considered to present the thermal efficiency of the MPSAH on different time of the day (from 8:30 to 16:30) for various mass flow rates on summer and winter seasons, respectively. As shown in Fig. 12 and Fig. 13, there is an increase in the thermal efficiency which resulted from increasing the mass flow rate from 0.0122 kg/s to 0.0130 kg/s for both seasons. But, for the summer season the maximum thermal efficiency was 70.42 %, and the maximum efficiency was 67.12% in the winter season for the flow rate of 0.0130 kg/s. This trend of the thermal efficiency behavior with the mass flow rates was similar to the recent studies that reported by Ekramian et al. [21] and Yousefi et al. [22]. Their research works were focused improving the heat transfer performance of flat plate solar collectors. It is also noted that in Fig. 12, the average efficiencies between 8:30 and 16:30 were 39.34%, 41.03%, and 43.19% for the flow rates of 0.0122 kg/s, 0.0127 kg/s, and 0.0130 kg/s, respectively. Similarly, in Fig.13 the average efficiencies between 8:30 and 16:30 were 37.44%, 38.16%, and 40.88% for the flow rates of 0.0122 kg/s, 0.0127 kg/s, and 0.0130 kg/s, respectively. However, it is noted that the average thermal efficiencies in summer season were higher than those in winter season for all values of mass flow rates examined.

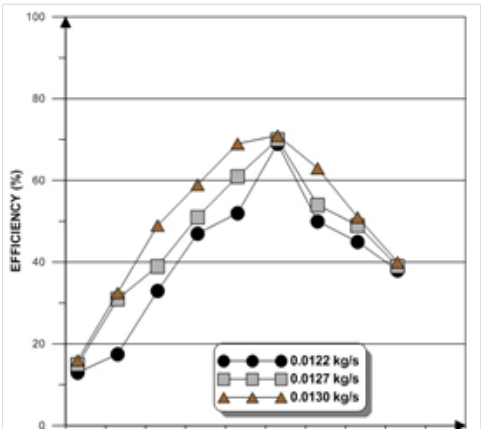

Figure 12: Thermal efficiency of the MPSAH on different time of the day with different mass flow rates on summer season.

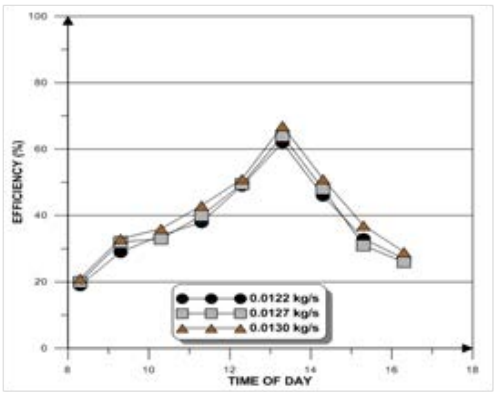

Figure 13: Thermal efficiency of the MPSAH on different time of the day with different mass flow rates on winter season.

The thermal efficiency of the MPSWH on various times (from 8:30 to 16:30) of the day with different mass flow rates (0.0165 kg/s, 0.0170 kg/s, and 0.0185 kg/s) on summer season is shown in Fig.14. The highest values of water heating efficiency were found at 12:30 pm, and they are 69%, 70%, and 71% for the sequence arrangement of aforementioned mass flow rates. Comparing to the efficiency of conventional SWH, which is not presented in this paper, the efficiency of the MPSWH is higher for the same values of mass flow rate and solar radiation. This is happened because of the substitution of thermal energy from the air heater, as mentioned earlier. On the winter season, the thermal efficiency of the MPSWH from 8:30 to 16:30 of the day with different mass flow rates is

presented in Fig.15. The maximum thermal efficiency of MPSWH for the following mass flow rates of 0.0165 kg/s, 0.0170 kg/s, and 0.0185 kg/s were 60%, 65%, and 69.5 %, respectively. As seen, the predicted results showed a clear change of the thermal efficiency of the MPSWH during the summer and winter seasons for the same values of mass flow rates adopted in this study. This can be caused to the reduction of the ambient temperature in the winter season with respect to that in summer season.

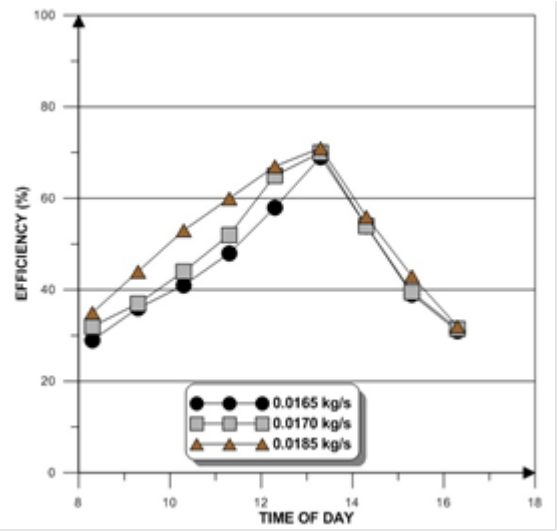

Figure 14: Thermal efficiency of the MPSWH on different time of the day with different mass flow rates on summer season

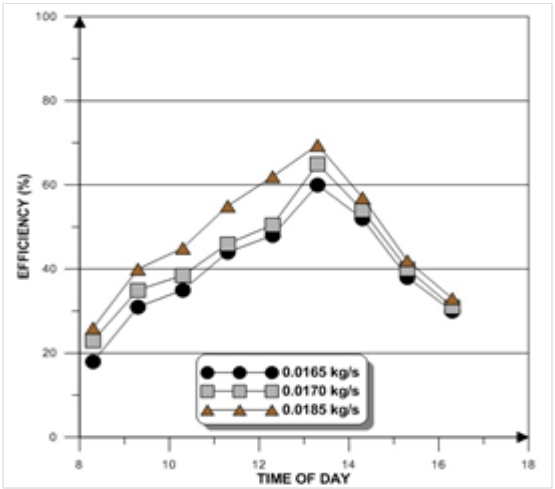

Figure 15: Thermal efficiency of the MPSWH on different time of the day with different mass flow rates on winter season

In addition to the effect of mass flow rate on the thermal performance of the MPSWH and MPSAH, an absorber material parameter has been also taken into consideration of the calculation. The absorber plate is one of the most important parameters in the solar flat plate collectors because the physical properties of absorber plate have a great importance on the conduction heat transfer phenomena. Three different materials of aluminum, copper, and steel with various thermal conductivities have been carried out for both the MPSWH and the MPSAH. In Fig. 16, the thermal efficiency of the MPSAH on various time of the day with three different absorber materials on the winter season is presented at the mass flow rate of 0.0122 kg/s. As seen, it is clear that by increasing the thermal conductivity of the absorber material the thermal efficiency increases. The percentage increases of average thermal efficiency of copper absorber plate are 7.60% and 43.69% higher than those of the aluminum and steel absorber plates, respectively. Regarding the MPSWH, the thermal efficiency on various time of the day with three different absorber materials on the winter season at the mass flow rate of 0.0165 kg/s is demonstrated in Fig.17. Based on the numerical results, the thermal efficiency of absorber plate is increased using the higher thermal conductivity of absorber materials. The percentage increases of average thermal efficiency of copper plate are up to 4.63% and 47.57% with respect to those of aluminum and steel absorber plates, respectively.

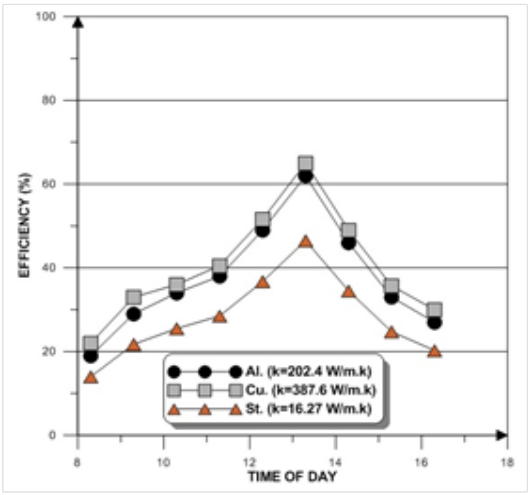

Figure 16: Thermal efficiency of the MPSAH on different time of the day with different absorber materials on winter season at mass flow rate of 0.0122 kg/s

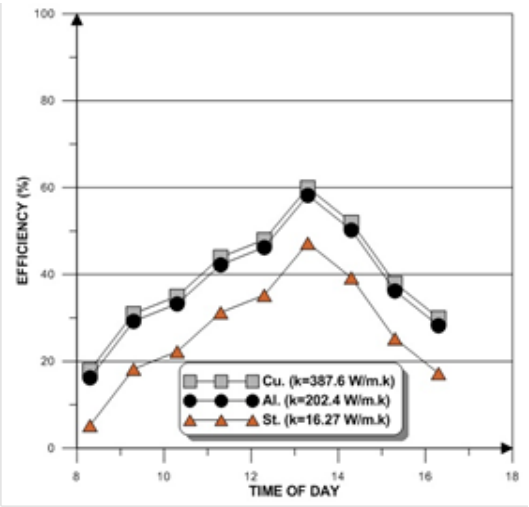

Figure 17: Thermal efficiency of the MPSWH on different time of the day with different absorber materials on winter season at mass flow rate of 0.0165 kg/s.

5. Conclusion

In order to optimize the thermal collectors in multipurpose solar heating systems, a computational fluid dynamics (CFD) modeling study has been carried out in the present paper. The study has involved solving continuity equation, momentum equation, and energy equation via a finite-volume CFD numerical package, AVL Fire CFD code ver. 2009.2, using the RNG k - ε turbulence model.

The 3-D computational domain of solar water heater and the 3-D computational domain of the solar air heater have been used for CFD analysis. The geometry of absorber plate and riser tube of both solar water and air heater have been created, and simulated. In multipurpose solar water heating (MPSWH) system, the simulated results have been compared with experimental data examined by Venkatesh and Christraj [15], and the discrepancies fall within 9.46% in summer season and 8.31% for winter season. In the same way for multipurpose solar air heating (MPSAH) system, the differences between the experimental and numerical results were 6.54% and 10.84% respectively, and it proves that the simulated results are within the acceptable limits. The increases in the temperature were 37 ^{o}C and 25 ^{o}C for the MPSWH and MPSAH, respectively in comparison with those of the conventional SWH and the conventional SAH. Both of the mass flow rates and absorber materials have been numerically investigated for the MPSWH and MPSAH as essential practical parameters in solar heating systems. The predicted results showed that there is an increase in the thermal efficiency of solar collectors with increasing the mass flow rates and the thermal conductivity of the absorber materials examined in summer and winter seasons. In short, the CFD modeling study can provide a wide range of efficient information to the design of solar heating systems before making any expensive and time-consuming experimental investigations.

References

[1] Vestlund, H., Dalenback, J., Ronnelid, M., 2012. “Thermal and mechanical performance of sealed, gas-filled, flat plate solar collectos”, Solar Energy 86, 13-25.

[2] Jinwei, Ma., Wei Sun., 2011.”Experimental and theoretical study of the efficiency of a dual -function solar collector”, Applied Thermal Engineering., 31, 1751-56.

[3] Gill, R. S., Sukhmeet Singh., 2012, “Low cost solar air heater”, Energy Conversion and Management ., 57, 131-42.

[4] Zhao, DL, Li, Y, Dai, YJ & Wang, RZ 2011, ‘Optimal study of a solar air heating system with pebble bed energy storage’, Energy Conversion Management vol. 52, pp. 2392–2400.

[5] Oliva A, Costa M, Perez Segarra C. 1991, "Numerical simulation of solar collectors: the effect of non-uniformity and non-steady state of boundary conditions. Sol Energy, 47 (5):359-373.

[6] Manjunath M, Karanth K, Sharma N. 2011, "Three dimensional numerical analysis of conjugate heat transfer for enhacement of thermal performance using finned tubes in an economical unglazed solar flat plate collector", Proc World Congress on Engineering. London (UK), III:2245-2249.

[7] Manjunath M, Karanth K, Sharma N. 2012, "A comparative CFD study on solar dimple plate collector with flat plate collector to augment the thermal performance", World Academy of Science, Engineering and Technology, 70: 969-975.

[8] Zima W, Dziewa, P. 2010, "Mathematical modeling of heat transfer in liquid flat-plate solar collector tubes", Arch Thermodyn, 31(2): 45-62.

[9] Zima W, Dziewa, P. 2011, "Modelling of liquid flat-plate solar collector operation in transient states", Proc Inst Mech Eng., Part A: J Pow Energy, 255(1): 53-62

[10] Budihardjo I, Morrison GL. 2009,"Performance of water-in-glass evacuated tube solar water heaters", Sol Energy, 89:49-56.

[11] Ayome LM, Duffy A, Mc Keever M, Conlon M, McCormack SJ. 2011, "Validated TRNSYS model for forced circulation solar water heating systems with flat plate and heat pipe evacuated tube collectors", Appl Therm Eng, 31: 1536-1542.
[12] Fan J, Shah L, Furbo S. 2007, "Flow distribution in a solar collector panel with horizontally inclined absorber strips", Sol Energy, 81: 1501-1511.
[13] Turgut O, Onur N. 2009, "Three dimensional numerical and experimental study of forced convection heat transfer on solar collector surface", Int Commun Heat Mass Transf, 36:274-279.
[14] Anonymous. AVL Fire CFD Solver v 8.5 manual, A-8020 Gras, Austria; 2009. <www.avl.com>.
[15] Venkatesh, R. and Christraj, W. 2015, "Experimental investigation of multipurpose solar heating system", *J. Energy Eng.*, 141 (3), 04014009.
[16] Patankar SV, Spalding DB. 1972, "A calculation procedure for heat, mass and momentum transfer in three-dimensional parabolic flows", Int J Heat Mass Transfer;15:1787–806.
[17] GJ. Hwang, CH.Chao, 1994, "Heat transfer measurement and analysis for sintered porous channels", J Heat Transfer; 116:456–64.
[18] G. Biswas, V. Eswaran, 2002, "Turbulent flows fundamentals experiments and modeling", New Delhi: Narosa publishing house.
[19] Versteeg HK, Malalasekera W. 2007," An introduction to computational fluid dynamics the finite volume method", Harlow [u.a]: Pearson/Prentice Hall.
[20] Bo-Ren, C, Yu-wei, C, Wen-Shing, L & Sih-Li, C 2009, 'Long term thermal performance of a two-phase thermosyphon solar water heater', solar energy, vol. 83, pp. 1048-1055.
[21] E. Ekramian, S. Gh. Etemad, M. Haghshenasfard, 2014,"Numerical analysis of heat transfer performance of flat plate solar collectors", Journal of Fluid Flow, Heat, and Mass Transfer; DOI:10.11159/jffhmt.2014.006
[22] Yousefi, T., Veisy, F., Shojaeizadeh, E., Zinadini, S., 2012, "An experimental investigation on the effect of MWCNT-H2O nanofluid on the efficiency of flat-plate solar collectors", Experimental Thermal and Fluid Science 39, 207–212.

دراسة نمذجة ديناميات الموائع الحسابية (CFD) للأداء الحراري لمنظومات التسخين الشمسي متعددة الاغراض

عدي حسين كاظم العباس
قسم هندسة تقنيات المضخات ،الكلية التقنية المسيب
جامعة الفرات الاوسط التقنية

الخلاصة:

ان المحاكاة العددية ثلاثية الابعاد للجامع الحراري في انظمة التسخين الشمسي قد نفذت لمحاكاة انظمة التسخين الشمسي التقليدي و انظمة التسخين الشمسي المائي متعدد الاغراض (MPSWH) و انظمة التسخين الشمسي الهوائي متعدد الاغراض (MPSAH).ان برنامج ديناميك الموائع الحسابية التجاري AVL Fire ver. 2009.2 (CFD) قد استخدم لحل وتفحص توزيعات درجات الحرارة في لوحة امتصاص وأنبوب الناهض في كل من MPSWH وMPSAH خلال فصل الصيف والشتاء. ان موديل الجريان الاضطرابي k - ε RNG قد وظف في هذه الدراسة العددية. ان الغاية من البحث الحالي هي للتزود بمعلومات جيدة لزيادة الاداء الحراري لمنظومات التسخين الشمسي في مختلف شروط العمل. قد تم استخدام البيانات العملية من المصدر [15] كمدخلات للبرنامج الحسابي. مقارنتا الى القيم العليا لدرجات الحرارة في منظومات التسخين المائي والهوائي التقليدية (SWH و SAH) ، كانت النتائج العددية ل MPSWHو MPSAH افضل على الاداء الحاري للمنظومة. هذه التحسينات على قيم درجات الحرارة حدثت بسبب التصميم الجديد المعتمد في أنظمة التدفئة الشمسية متعددة الأغراض باستخدام أنابيب الناهض والرؤوس إلى التصميم الأصلي للأنظمة الحرارية. بالإضافة إلى ذلك، فإن الأداء الحراري لجامع الطاقة الشمسية يزداد مع زيادة معدلات التدفق والتوصيل الحراري من لوحة الامتصاص. لغرض التحقيق من النتائج العددية، أظهرت النتائج المتوقعة لجميع الحالات التي تم فحصها اتفاق جيد ضد النتائج العملية من حيث مستويات توزيع درجة الحرارة والكفاءة الحرارية.